Theoretical and Applied Climatology (2022) 150:1131–1144
https://doi.org/10.1007/s00704-022-04212-3

ORIGINAL PAPER

An interdecadal enhancement of relationship between Northwest and North China summer precipitation since early 2000

Zhaoyang Du[1,2,3,4] · Lian-Tong Zhou[1] · Xiaoxue Yin[5]

Received: 28 December 2021 / Accepted: 13 September 2022 / Published online: 30 September 2022

Abstract

The present study investigates a significant enhancement in the relationship between summer precipitation in Northwest China (NWC) and that in North China (NC) (the NWC and NC region) after early 2000, using the CN05.1 dataset and the NCEP-NCAR reanalysis circulation data from 1961 to 2018. The change in the relation between summer precipitation variations in these two regions after early 2000 likely relates to the change of the wave trains in mid-high latitudes. Before 2000, atmospheric circulation anomalies associated with the summer precipitation in NWC resemble the Silk Road Pattern (SRP) and the British-Baikal Corridor (BBC) pattern, but that in NC only resembles the SRP. After 2000, the summer precipitation in NWC and NC has a significant positive correlation with the BBC pattern. The BBC pattern influences summer precipitation in NWC and NC after early 2000 through the Ural blocking high, the positive 500-hPa *Z* anomalies over the Mediterranean Sea and Northwest Pacific, and the East Asia trough that leads the cold air to the south. These four synoptic systems co-modulate the summer precipitation in NWC and NC. In addition, when NWC has the same (opposite) sign as NC summer precipitation, there is BBC (SRP) wave train across Eurasia at high (middle) latitudes.

1 Introduction

Northwest China and North China are located in the arid and semi-arid region of East Asia, with an ecological balance and economic development that are highly sensitive to climate change (Liu et al. 2005; Mo et al. 2016). Precipitation variation over Northwest China (Li et al. 2003; Shi et al. 2003; Song and Zhang 2003; Wang et al. 2003; Wei et al. 2010; Zhao et al. 2014; Li et al. 2016; Liu et al. 2017; Peng and Zhou 2017; Zhang et al. 2019) and North China (Yang et al. 2005, 2020; Tang and Lin 2007; Liu and Ding 2011; Hao and Ding 2012), which can cause severe natural disasters, thus threatening human lives and properties, is among the most concerning climate change issues in Northern China (Huang et al. 2013, 2019; Zhang et al. 2020). Therefore, studying the climate change characteristics in these two regions has a crucial scientific significance for disaster prevention and mitigation and optimization of environmental quality.

There may be connections in the climate in different regions (Wu 2002, 2017; Zhou and Chan 2007; Lin et al. 2017; Li et al. 2021), which are related to large-scale circulation (Huang et al. 2008; Gong et al. 2018). Huang et al. (2008) showed that the interaction between the Eurasian (EU) pattern and the East Asia–Pacific (EAP) pattern enhances the sensible heat in Northwest China and then reduces the summer precipitation in North China. Gong et al. (2018) found that the spatial distribution of summer precipitation anomalies in the East Asia-West Pacific region corresponds to the phase of EAP teleconnection and Silk Road teleconnection. The Silk Road Pattern (SRP), a well-known teleconnection model of the westerly jet along the upper Eurasian continent in summer, has a significant impact

Revised manuscript was submitted for *Theoretical and Applied Climatology* on September 3, 2022.

✉ Lian-Tong Zhou
zlt@mail.iap.ac.cn

[1] Center for Monsoon System Research, Institute of Atmospheric Physics, Chinese Academy of Sciences, P.O. Box 2718, Beijing 100190, China

[2] Key Laboratory for Meteorological Disaster Monitoring and Early Warning and Risk Management of Characteristic Agriculture in Arid Regions, CMA, Yinchuan 750002, China

[3] Ningxia Key Laboratory for Meteorological Disaster Prevention and Reduction, Yinchuan 750002, China

[4] Ningxia Meteorological Observatory, Yinchuan 750002, China

[5] Department of Navigation, China Coast Guard Academy, Ningbo 315801, China

on the summer climate of Eurasia (Lu et al. 2002; Huang et al. 2011; Kosaka et al. 2011; Wang et al. 2017a; Liu et al. 2020). The SRP and dipoles across the North Atlantic are the dominant patterns of precipitation change in Northwest China in July (Chen and Huang 2012). The interannual variations of June–September mean rainfall in North China are well related to the upper-level circumglobal teleconnection (CGT) in boreal summer, which is similar to SRP at least over the Eurasian continent (Ding and Wang 2005; Li et al. 2019; Zhou et al. 2019). Besides, the British-Baikal Corridor (BBC) pattern, which is the wave train over the Eurasian continent in the high-latitude area where the polar jet is located, impacts the area's climate along the route (Xu et al. 2018). However, the relationship between regional precipitation and atmospheric circulation is unstable (Liu et al. 2020; Yin and Zhou 2020). Yin and Zhou (2020) found the correlation between winter precipitation in Northwest China and ENSO, and the mid-latitude North Atlantic sea surface temperature strengthened after the mid-1990s. The SRP has interdecadal changes around the late 1970s and late 1990s, corresponding to the precise shifts of the summer climate over Eurasia (Liu et al. 2020). The meridional characteristics of summer precipitation in Eastern China have been extensively studied in the past (Nitta 1987; Huang 2004; Chen and Zhai 2015; Sun et al. 2019; Shang et al. 2020). There are also some researches about how latitude affects the summer precipitation in Northwest and North China (Yu et al. 2003; Zhou and Huang 2006; Tang and Lin 2007; Chen and Dai 2009; Zhao et al. 2011; Wang et al. 2013, 2017b; Liu et al. 2017). In Northwest and North China, summer precipitation has opposite trends (Shi et al. 2003; Zhou and Huang 2006; Tang and Lin 2007; Wang et al. 2013, 2017b; Li et al. 2016; Peng and Zhou 2017). For instance, there has been a persistent drought in North China since the 1970s (Huang et al. 1999; Zhou and Huang 2003; Liu and Ding 2011; Hao and Ding 2012; Han et al. 2019); the summer rainfall in Northwest China was relatively high after the 1980s, and the climate changed from warm and dry to warm and wet (Shi et al. 2002; Ren and Yang 2007; Liu et al. 2011). In addition, the summer precipitation in Northwest China shows noticeable regional differences, which is increasing in the east and decreasing in the west (Yu et al. 2003; Chen et al. 2009; Liu et al. 2017; Zhao et al. 2017). Zhang et al. (2019) suggested that a seesaw phenomenon in the east and west parts of Northwest China during flood season is related to the reverse phase relationship between the East Asian summer monsoon index and the westerly circulation index.

The above studies have focused on climate change in Northwest and North China. However, few have analyzed the relationship between the summer precipitation variabilities in these two regions, which involve the interaction between monsoon and non-monsoon regions. Has the relationship between summer precipitation in Northwest China and that in North China changed? Moreover, what are the possible mechanisms from the internal variability of the climate system? These questions will be addressed in this study. Therefore, we present evidence to demonstrate that there was indeed an interdecadal change in the relationships between summer (June–August (JJA)) precipitation in these two regions and its possible causes from the mid-latitude circulation system. Understanding the interdecadal changes in the relationship between the JJA precipitation in Northwest and that in North China has critical scientific implications for improving the regional precipitation prediction.

The remainder of this paper is organized as follows: The datasets and methods used in this paper are described in Sect. 2. In Sect. 3, interdecadal change in the linkage between summer precipitation in Northwest China and that in North China is presented. Section 4 describes the atmospheric circulation anomalies related to the interdecadal change in the correlation between the summer precipitation in Northwest China and that in North China. Finally, Sect. 5 provides a summary and discussion.

2 Data and method

The following datasets are extensively used in our analyses: (1) the monthly precipitation data over China use the CN05.1 data, with a $0.25° \times 0.25°$ resolution, using the software package ANUSPLIN developed by the Australian National University, and it is derived from precipitation data interpolation of more than 2000 stations in China (Wu and Gao 2013); (2) the monthly precipitation data from the Climatic Research Unit (CRU) high-resolution gridded datasets, version 4.04 with $0.25° \times 0.25°$ resolution (CRU TSv4.00; Harris et al. 2014); and (3) the monthly atmospheric reanalysis datasets from the National Centers for Environmental Prediction and National Center for Atmospheric Research (NCEP-NCAR), with $2.5° \times 2.5°$ horizontal resolution (Kalnay et al. 1996).

We mainly focus on the summer precipitation in our study. The SRP teleconnection index (SRPI) is defined in the standardized principal component (PC) corresponding to the first leading mode (empirical orthogonal function 1 (EOF1)) of the summer 200-hPa meridional wind (V200) anomalies over the domain 20–60° N, 0–150° E (Liu et al. 2020). Similar to the definition of SRPI, the BBC teleconnection index (BBCI) is defined in the standardized PC corresponding to the EOF1 of the 250-hPa meridional wind over the domain 50–80° N, 20° W–150° E (Xu et al. 2018).

In order to analyze the variation characteristics of the element field at different scales, it is necessary to select a filter to filter the variables. The Butterworth filter is a filter with the smoothest frequency response curve of a passband proposed by British engineer Stephen Butterworth. Low-pass

filtering is used to extract interdecadal signals, and high-pass filtering is used for interannual signals. The higher the order, the smoother it is. The principle is as follows:

$$|H(\omega)|^2 = \frac{1}{1+(\frac{\omega}{\omega_c})^{2n}} = \frac{1}{1+\epsilon^2(\frac{\omega}{\omega_p})^{2n}}$$

where n is the order of the filter, ω_c is the cutoff frequency, that is, the frequency when the amplitude drops to − 3 dB; ω_p is the frequency of the edge of the passband; and $\frac{1}{1+\epsilon^2}$ represents the value of $|H(\omega)|^2$ at the edge of the passband. We construct a 1st-order Butterworth high-pass filter to extract the interannual signals of the standardized summer precipitation series in Northwest China (NWC) and North China (NC), and define the high-frequency variation with a period of less than 10 years as the interannual part, and the sampling frequency is 1 year. The decadal period is 10 years, then the frequency is 0.1, and the cutoff frequency is = 2 × 0.1/1 = 0.2.

The period time is 1961–2018 for all the datasets. In this paper, the correlation, regression, and composite analysis are used, and the two-tailed Student's t test is used to estimate the significance.

3 Interdecadal change in the linkage between summer precipitation in NWC and that in NC

From the internal climatology, Northwest and North China involve the interaction of non-monsoon and monsoon regions. This interaction makes these two regions inseparable. Huang et al. (2011) pointed out the apparent difference in precipitation between the east and the west of Northern China, and their dividing line is around 100° E. Wang et al. (2012) showed that the second EOF mode of summer precipitation in arid and semi-arid regions of East Asia is an east–west contrast pattern and divides the arid/semi-arid areas by the 100° E meridian. Besides, we further find that the second EOF mode of summer precipitation variability in the two regions presents a dipole near 100° E (not shown). Therefore, we first divide NWC and NC by 100° E (Fig. 1a).

Figure 1b shows the mean summer rainfall anomalies averaged over NWC (blue dotted line) and NC (red dotted line) using the CN05.1 dataset. Consistently, after early 2000, the time series of the summer precipitation in NWC and NC increase simultaneously. Some prior studies find that precipitation in NC begins to increase after early 2000 (Yang et al. 2017, 2021; Ma et al. 2020). In order to better reflect the interdecadal transition of the relationship between NWC and NC summer precipitation, we use a 1st-order Butterworth filter to filter out the interdecadal signals of the summer precipitation series in these regions. The filtered series

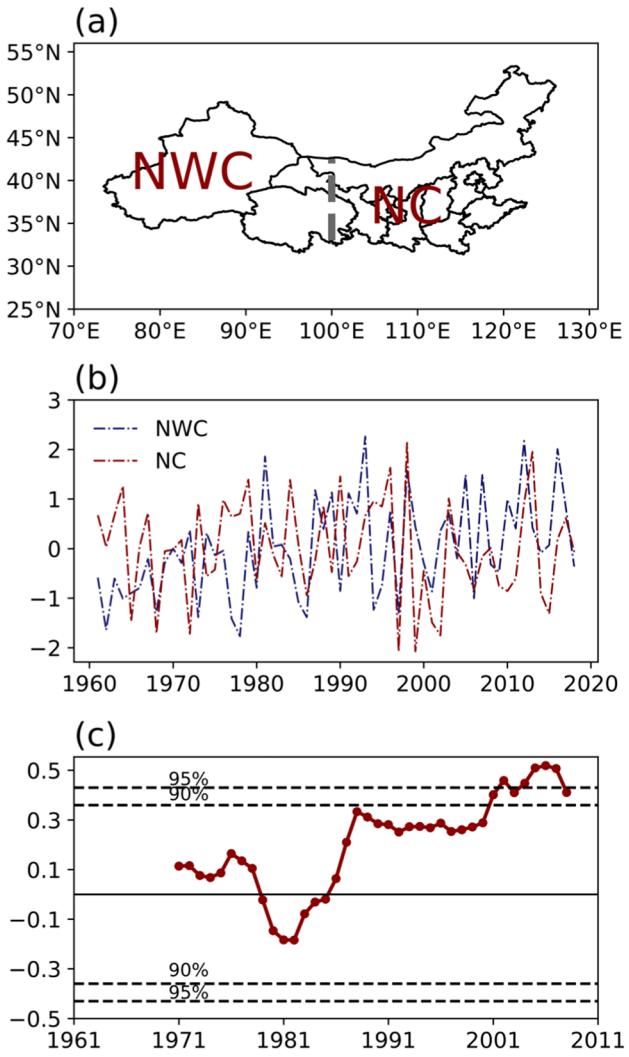

Fig. 1 **a** Region map of Northwest China (NWC) and North China (NC). **b** The standard time series of summer precipitation in NWC (blue dashed line) and NC (red dashed line) for the period 1961–2018 (unit: mm/day). **c** Moving correlation coefficient between the NWCI and NCI with a 21-year window. The correlation is shown at the center year of the 21-year window. Horizontal dashed lines indicate the correlation coefficient is significant at the 90% and 95% confidence levels

is defined as the summer precipitation index in NWC and NC (NWCI and NCI). Years labeled in Fig. 1c denote the central year of the 21-year window. The positive correlation became enhanced after the mid-1980s, but the correlation coefficients (CCs) were small and insignificant before early 2000. After early 2000, the correlation strengthens notably, and the CCs get largely positive and significant. In the following analyses, two periods before and after 2000 were selected according to the sliding correlation in Fig. 1c to investigate the interdecadal change. To clearly illustrate the correlation between summer precipitation in NWC and that in NC around early 2000, two periods (1973–1991 (P1),

2000–2018 (P2)) were selected. The results obtained in this study are not sensitive to the reasonable change (forward or backward by several years) of the selected two periods. The correlation coefficient between the area-averaged NWC and NC summer precipitation is − 0.17 during P1 and reaches up to 0.42 during P2. Thus, the selection of the two periods (P1 and P2) is reasonable.

4 Factors for the interdecadal change between summer precipitation in NWC and that in NC

We further investigate underlying factors that the interdecadal change in the NWC-NC summer precipitation relationship. Atmospheric circulation anomalies are first examined. The connection of precipitation in the two remote regions is likely related to atmospheric circulation patterns. Fig. 2a and b exhibits the regression maps of 200-hPa meridional wind (V200) anomalies with NWCI for periods P1 and P2. During P1, there were two markedly anomalous wave trains in mid-latitudes and high latitudes at V200, respectively. The former has four anomalous centers over West Asia, Central Asia, North China, and Japan. Primarily, there is a positive anomaly over NWC. This structure resembles the negative SRP pattern, which is the first leading mode of the summer V200. However, the latter is a BBC-like pattern, with four anomalous centers over North-Central Atlantic, western Siberia, southern Barents Sea, and western Okhotsk Sea. These illustrate that the summer precipitation in NWC for P1 is related to the SRP pattern and BBC pattern. During P2, the anomalous wave train in mid-latitude at V200 is weakened, and only one negative anomaly is located in the Black Sea. Besides, a negative anomaly over the Greenland Sea is stronger, but the Eurasian continent's anomalies are slightly weaker than P1. Concerning the NCI (Fig. 2c, d), V200 anomalies show an SRP-like pattern in mid-latitude during P1. This structure's four notable anomalous centers are located over the Caspian Sea, Central Asia, North China, and Japan. However, it weakens considerably during P2, and only one negative anomaly located over Japan intensifies and moves northward. In addition, a BBC-like pattern in high latitude is stronger during P2 than during P1, which stretches across much of the Eurasian continent. Therefore, we can hypothesize that the change in the relation between summer precipitation variations in the two regions after early 2000 likely relates to the change of the wave trains in mid-high latitude.

According to the above analysis, we have found that the large-scale circulation systems related to the summer precipitation in NWC and NC are SRP and BBC. Thus, we calculate the CCs between summer precipitation in these two regions and these two patterns further our understanding of their relationships in different periods (Table 1). During P1, the CC between SRPI and NWCI is − 0.59, and the CC with NCI is 0.59, both exceeding the 99% statistical confidence level. After 2000, the NWCI and NCI are weakly correlated with SRPI, with CCs of − 0.02 and − 0.29, respectively, but are closely related to BBCI, with CCs of 0.49 and 0.69 (both exceeding the 99% confidence level). There is no significant connection between NCI and BBCI during P1, only − 0.1,

Table 1 Correlation coefficients between the summer precipitation index (NWCI and NCI) and SRP index (SPRI) and BBC index (BBCI) during 1973–1991 and 2000–2018

	SRPI		BBCI	
	1973–1991	2000–2018	1973–1991	2000–2018
NWCI	− 0.52*	− 0.02	0.52*	0.49*
NCI	0.59*	− 0.29	− 0.1	0.69*

Numbers with an asterisk indicate the values above the 99% statistical confidence level

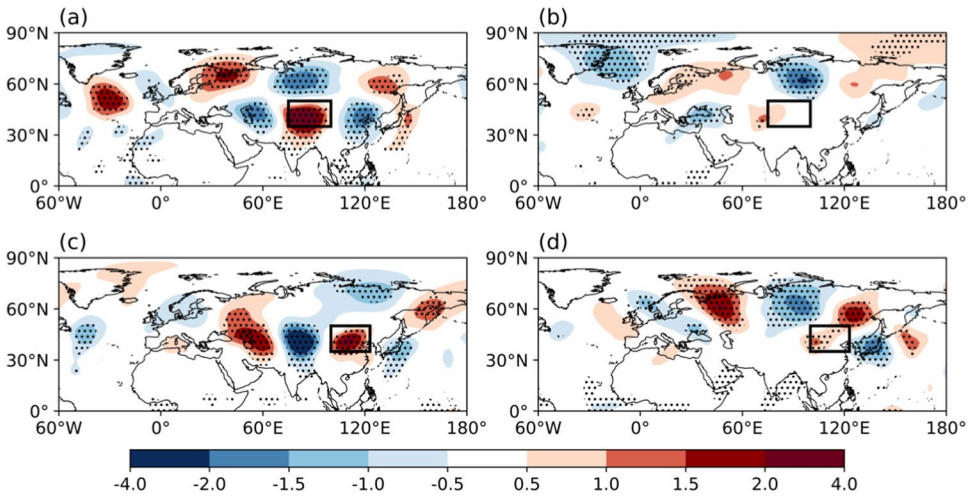

Fig. 2 Regression maps of anomalies of JJA meridional wind at 200 hPa (units: m/s) with NWCI (**a**, **b**) and NCI (**c**, **d**) in 1973–1991 (left) and 2000–2018 (right). Dotted regions indicate the 95% confidence level, based on Student's *t* test. The boxes in **a** and **b** and in **c** and **d** denote the locations of NWC and NC, respectively

but the CC between NWCI and BBCI is 0.52 (exceeding the 99% confidence level). The statistical results are similar to Fig. 2. In brief, the summer precipitation in NWC is both related to SRP and BBC, but that in NC is only related to SRP. After 2000, the summer precipitation in NWC and that in NC are only related to BBC, which may be one of the reasons for the significant positive correlation between the summer precipitation in NWC and NC.

We then use a 0.5 standard deviation (SD) as the criterion to choose the years for composite analysis. When both the NWCI and NCI of a year are positive (negative) and one is larger (less) than 0.5 (−0.5) SD, this year is categorized as the same-sign year (Table 2). When both the NWCI and NCI of a year are opposite and one of them is larger than 0.5 or less than −0.5, this year is categorized as the opposite-sign year. There are 7 same-sign years and 12 opposite-sign years during P1, but 13 same-sign years and 5 opposite-sign years during P2. These demonstrate an enhanced positive connection between the summer precipitation in NWC and that in NC, consistent with Fig. 1c. At V200 field (Fig. 3), when NWC has the same (opposite) sign as NC summer precipitation, there is BBC (SRP) wave train across Eurasia at high (middle) latitudes.

Figure 4 exhibits the 500-hPa geopotential height (Z) and 850-hPa wind anomalies obtained by regression on the NWCI and NCI during the two epochs. The 500-hPa Z anomaly associated with summer precipitation anomaly

Table 2 Years selected for the composite analysis

	1973–1991	2000–2018
Same sign	1976 (+), 1979 (+), 1980 (−), 1981 (+), 1985 (−), 1986 (−), 1988 (+)	2000 (−), 2001 (−), 2002 (−), 2003 (+), 2006 (−), 2007 (+), 2009 (−), 2012 (+), 2013 (+), 2014 (−), 2015 (−), 2016 (+), 2017 (+)
Opposite sign	1973, 1974, 1975, 1977, 1978, 1982, 1983, 1984, 1987, 1989, 1990, 1991	2004, 2005, 2008, 2010, 2011, 2018

The "+" and "−" signs denote the NWCI and NCI are both positive and negative, respectively

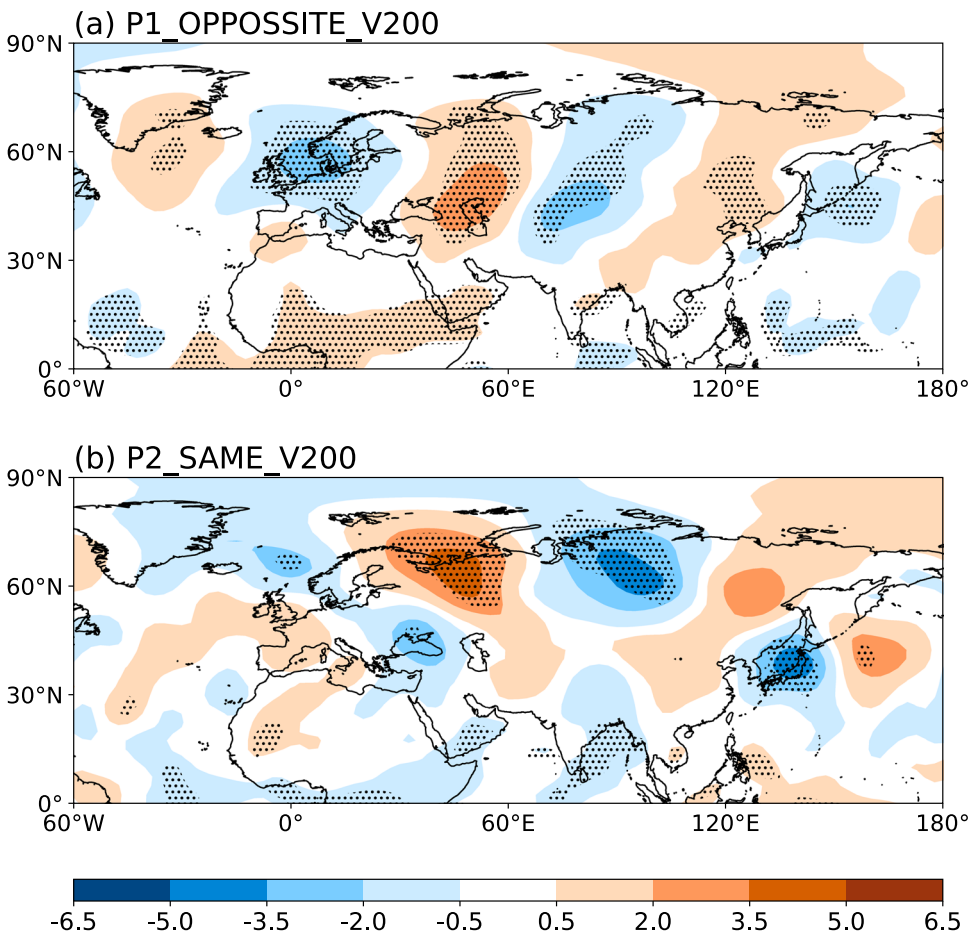

Fig. 3 Composite maps of JJA meridional wind at 200 hPa (units: m/s) for **a** opposite-sign years during P1 and **b** same-sign years during P2. Dotted regions indicate the 95% confidence level, based on Student's *t* test

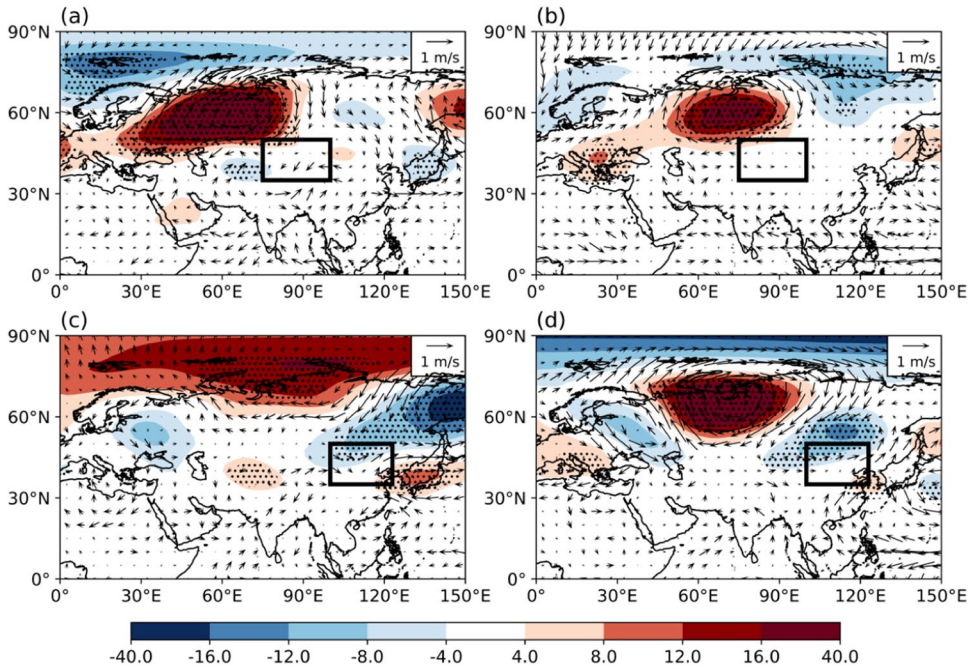

Fig. 4 Regression maps of anomalous JJA 500-hPa geopotential height (shading, units: gpm) and 850-hPa wind (vector) (units: m/s) with respect to **a**, **b** NWCI and **c**, **d** NCI for the periods 1973–1991 (left) and 2000–2018 (right). Dotted regions indicate the regression coefficients for geopotential height are significant at the 95% confidence level using the two-tailed Student's *t* test. The boxes in **a** and **b** and in **c** and **d** denote the locations of NWC and NC, respectively

in NWC for P1 shows a significant positive anomaly over the southern Kara Sea, accompanying two negative *Z* anomalies extending from the Caspian Sea to NWC and over the Japan Sea (Fig. 4a). Anomalous upward motion around NWC is shown in Fig. 5a. The low pressure, associated cyclonic anomalies (Fig. 4a), and concurrent anomalous upward motion over NWC are responsible for more precipitation in situ (same as Fig. 1b). The source of water vapor in NWC is mainly transported from the southwest (Fig. 6a). This water vapor transport anomaly is consistent with circulation and wind anomalies. Southwesterly wind anomalies can transport water vapor from the Indian Ocean to NWC and huge anticyclonic circulation over the Ural Mountains can transport water vapor from the Atlantic to NWC, making NWC to have more precipitation in summer. During P2 (Fig. 4b), there are two positive anomalies over the Mediterranean Sea and the Ural Mountains, with a negative anomaly over eastern Siberia. Anomalous atmospheric signals over the Ural Mountains and the Mediterranean Sea, which stimulate the downstream dispersion of Rossby wave energy, can cause the negative *Z* anomaly around NWC with an anomalous upward motion (Li et al. 2021). Moreover, the southeast wind anomaly in the equatorial Pacific is significantly stronger during P2 than that during P1, which can bring moist air from low latitude to NWC. Water vapor transport associated with NWC and NC summer precipitation presents an anomalous anticyclone near the Ural Mountains during P2 (Fig. 6b, d). Its location is around 60° N. Besides, high latitudes show a wave train across Eurasia. The water vapor transport in NWC is weaker than that in the P1 stage (Fig. 6a). Anticyclonic circulation in the Ural Mountains can transport water vapor from the Atlantic to NWC. The water vapor transport in the Northwest Pacific is more active than that during the P1 stage. The northeasterly wind anomaly on the east side of the anomalous anticyclone over the Ural Mountains and the southeasterly wind anomaly from the Northwest Pacific converge in NC, which is favorable for increased precipitation (Fig. 6d). For the summer precipitation in NC, a significant negative 500-hPa *Z* anomaly extends from eastern Siberia to Northern China during P1 (Fig. 4c), leading to much cold and dry air to the south. The NC region is dominated by westerly anomalies at 800 hPa and anticyclone at 500 hPa. Accordingly, less precipitation occurs over NC during P1. The northeast wind anomaly from the polar region can transport cold and moist air from the Arctic Ocean to NC. The southeasterly winds from the Pacific are unusually weak, and less water vapor reaches NC. The positive *Z* anomaly over the Kara Sea during P2 is enhanced evidently (Fig. 4d). It forms an intense anticyclone center in the northern Eurasian continent, while to its east, there is a westward low-pressure trough. This trough forms a closed low pressure around NC. In addition, significant positive *Z* (i.e., high pressure) anomalies appear on the eastern coast of China, which is associated with the positive *Z* anomalies over the Mediterranean Sea and the Ural Mountains. The northward winds on the west side of this anomaly bring moist air from low-latitude areas and promote a northward advance of the East Asian monsoon rain belt (Wang and Ding 2008). All these circumstances contribute to more precipitation over NC. We mainly concentrate on the general circulation patterns obtained by regression on the NWCI and NCI during the two epochs.

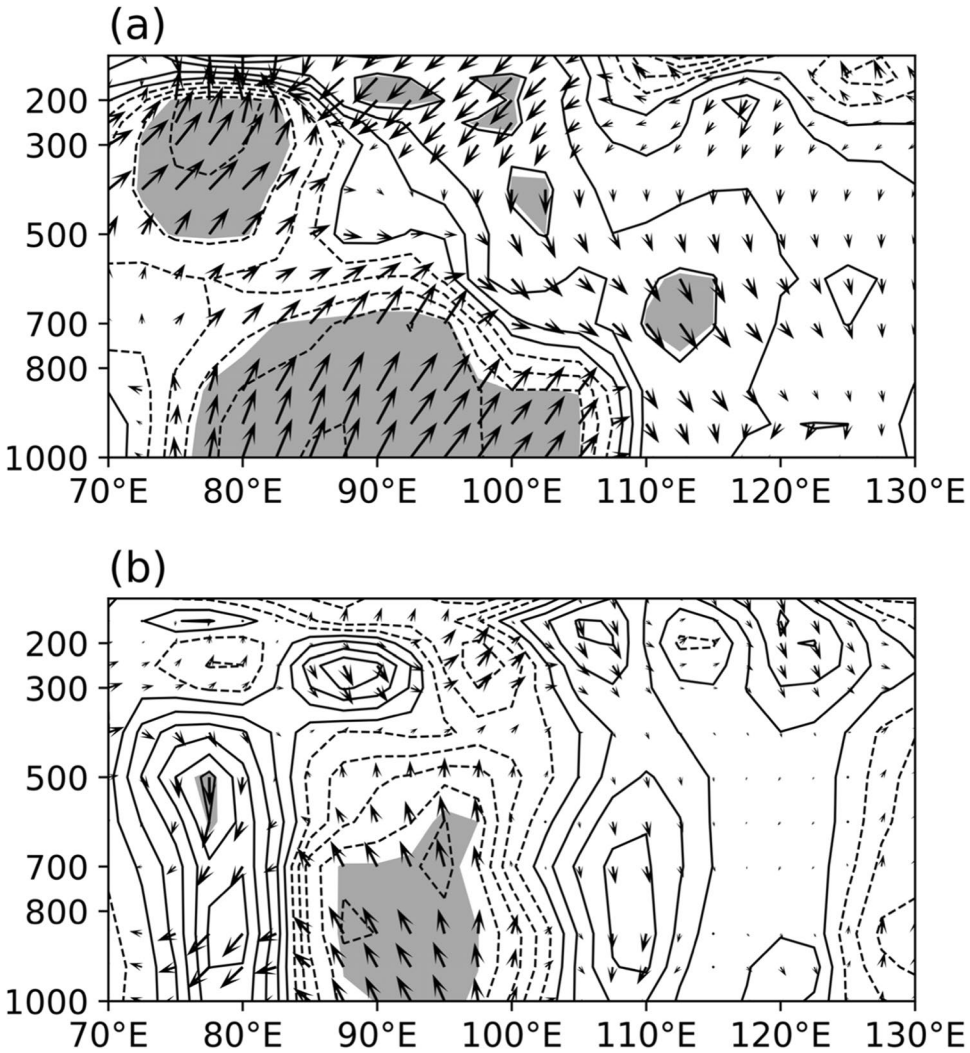

Fig. 5 Regression maps of anomalous JJA omega (contour, contour interval = 0.15, units: m/s) and vertical circulation (vector, synthesis based on u wind and omega, units: m/s) on a longitude-height cross section along 40° N with respect to NWCI for the periods **a** 1973–1991 and **b** 2000–2018. Shadings indicate the regression coefficients for omega are significant at the 95% confidence level using the two-tailed Student's *t* test

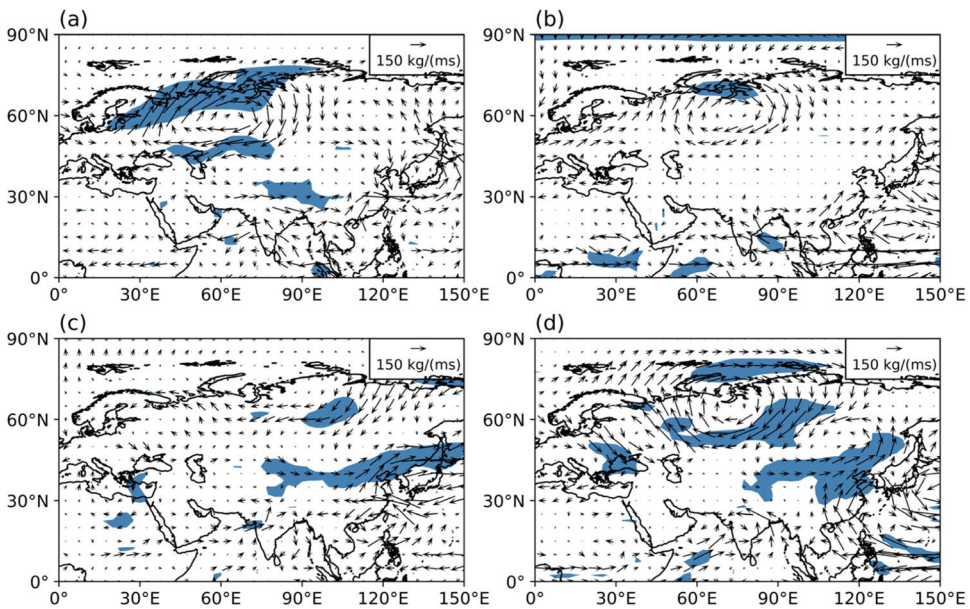

Fig. 6 Regression maps of anomalous JJA water vapor flux (vector, units: kg/ms) with respect to **a**, **b** NWCI and **c**, **d** NCI for the periods 1973–1991 (left) and 2000–2018 (right). Shading indicates the regression coefficients for JJA water vapor flux are significant at the 95% confidence level using the two-tailed Student's *t* test

In general, the mid-latitude structure of 500-hPa *Z* anomalies regressed by NWCI and NCI is opposite during P1 (Fig. 4a, c). There are striking differences in the locations and strength of the positive anomalous centers in high latitude. At 850 hPa, NWC has the northeast wind anomalies and NC has southwest wind anomalies. During P2 (Fig. 4b, d), there are two significantly positive anomalous centers located in the Mediterranean Sea and the Ural Mountains, which are part of the high-latitude wave train. At 850 hPa, NWC and NC have westerly anomalies. These results imply that anomalous atmospheric signals over the Ural Mountains and the Mediterranean Sea co-affect the positive *Z* anomaly near the eastern coast of China, accompanied by cold air from the north and wet air from the south, and then lead to the summer precipitation in NWC and NC which increased in coordination after early 2000.

Figure 7 shows the regression coefficients of meridional wind anomalies at 200 hPa with SRPI and BBCI in P1 and P2. NWC and NC have an inverse relationship during P1 with a significant positive anomaly over NWC and a significant negative anomaly over NC (Fig. 7a). Compared to that during P1, the SRP wave train during P2 significantly weakens and moves eastward (Fig. 7c). The atmospheric circulation anomalies related to the SRPI for the two periods are shown in Fig. 8. Previous studies suggested that SRP moves significantly eastward after the 1970s and is affected by high-latitude anomalies (Liu et al. 2020). We compared the SRPI-related circulation anomalies with the circulation anomalies related to the NWCI and NCI during the two epochs. During P1 (Fig. 8a), negative, positive, and negative *Z* anomalies are alternatively observed over Eurasia at mid-latitudes, which are similar to the structure obtained by

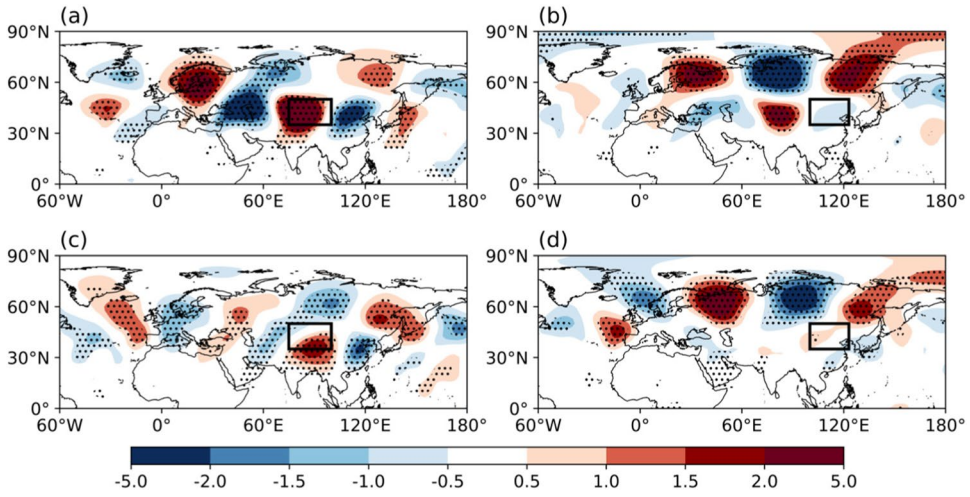

Fig. 7 Regression maps of meridional wind anomalies at 200 hPa (units: m/s) with SRPI (left) and BBCI (right) in 1973–1991 (**a**, **b**) and 2000–2018 (**c**, **d**). Dotted regions indicate the 95% confidence level based on Student's *t* test. The black boxes denote the locations of NWC and NC

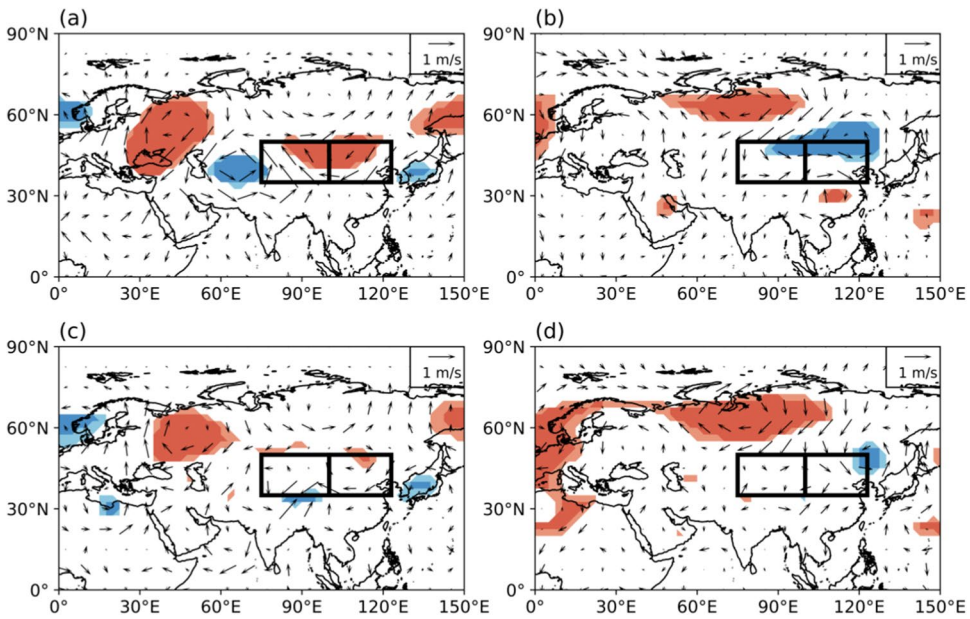

Fig. 8 Regression maps of anomalous JJA 500-hPa (**a**, **b**) and 850-hPa (**c**, **d**) geopotential height (shading, units: gpm) and wind (vector, units: m/s) with respect to SRPI for the periods 1973–1991 (left) and 2000–2018 (right). Deep and shallow shadings indicate the regression coefficients for geopotential height significant at 95% and 90% confidence levels using the two-tailed Student's *t* test. The boxes denote the locations of NWC (left) and NC (right)

regression on NWCI (Fig. 4a) and opposite to NCI (Fig. 4c). At 850 hPa (Fig. 8c), NWC and NC have easterly anomalies. The result is same as the SRPI-related water vapor transport (Fig. 9a). In contrast, the SRP is weakened during P2 (Fig. 8b, d), which is consistent with the result obtained by Liu et al. (2020). The corresponding positive centers occur in the two regions. After 2000, the Atlantic and the Kara Sea had two significant negative anomalous centers that tilted westward tilt height. This is consistent with the previous finding that significant circulation anomalies have occurred in Europe in recent decades (Wu 2002). One crucial difference is the location of the corresponding precipitation anomalies. Fig. 10a shows the correlation of the SRPI with precipitation anomalies for period P1. A negative correlation appears in the west of NC, whereas a positive correlation is observed in NWC. The correlation in this region is significant at the 95% confidence level. However, during P2 (Fig. 10b), the correlation of the SRPI and the summer precipitation decreases sharply. Here, the SRP may mainly affect the summer rainfall in NWC and NC during P1, which resembles that in Table 1.

The BBC wave train during P2 intensifies southward, and it distributes along the latitude of 60° N from the Atlantic Ocean to the Pacific Ocean (Fig. 7b, d). We compared the BBCI-related circulation anomalies with the circulation anomalies related to the NWCI and NCI during the two epochs (Fig. 11). The high-middle latitude anomalies at 500 hPa during P1 are centered mainly the Ural Mountains and the west of NWC during P1, which are similar to the NWCI-related circulation anomalies

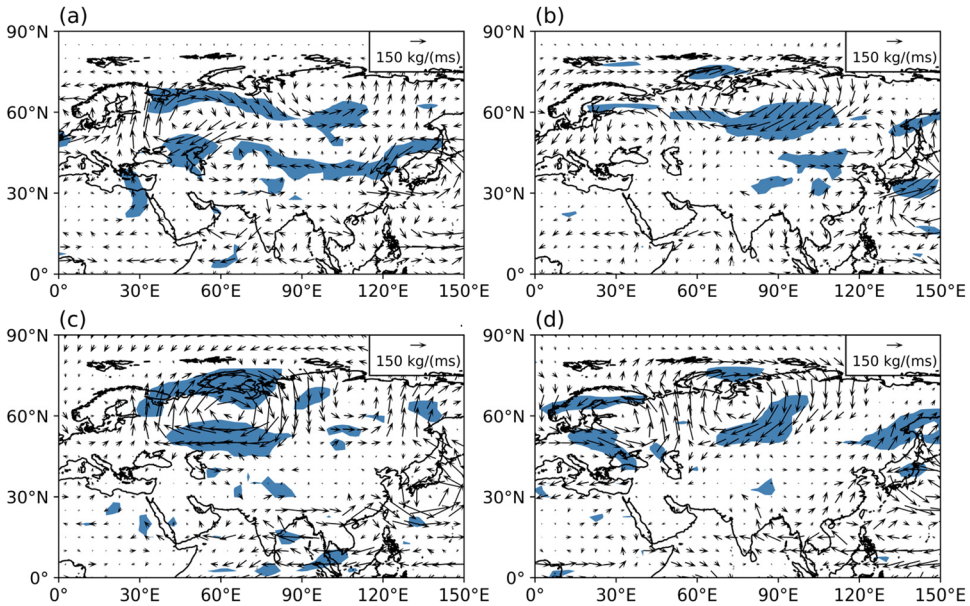

Fig. 9 Regression maps of anomalous JJA water vapor flux (vector, units: kg/ms) with respect to **a**, **b** SRPI and **c**, **d** BBCI for the periods 1973–1991 (left) and 2000–2018 (right). Shading indicates the regression coefficients for JJA water vapor flux are significant at the 95% confidence level using the two-tailed Student's *t* test

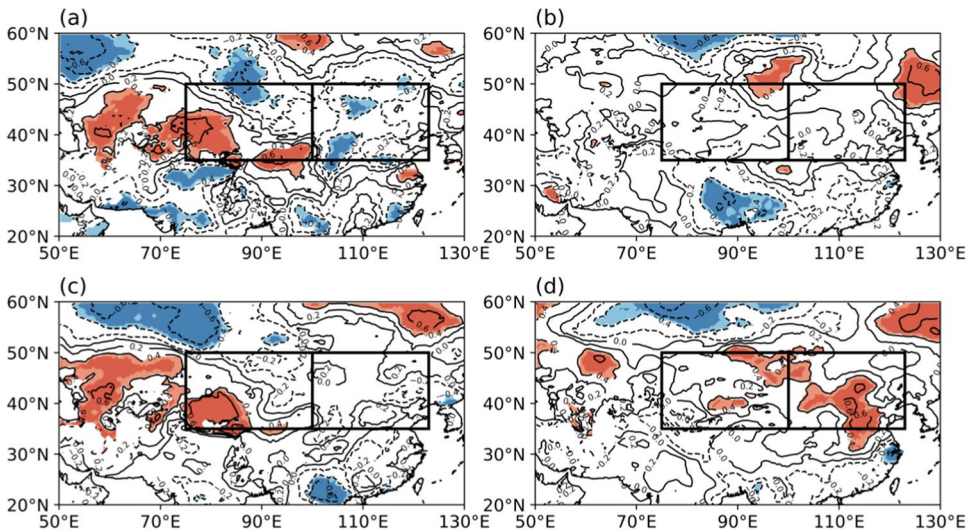

Fig. 10 Correlation maps of JJA precipitation anomaly (contour, contour interval = 0.2) with respect to **a**, **b** SRPI and **c**, **d** BBCI for the periods 1973–1991 (left) and 2000–2018 (right). Deep and shallow shadings indicate 95% and 90% confidence levels, separately. The boxes in **a** and **b** and in **c** and **d** denote the locations of NWC (left) and NC (right)

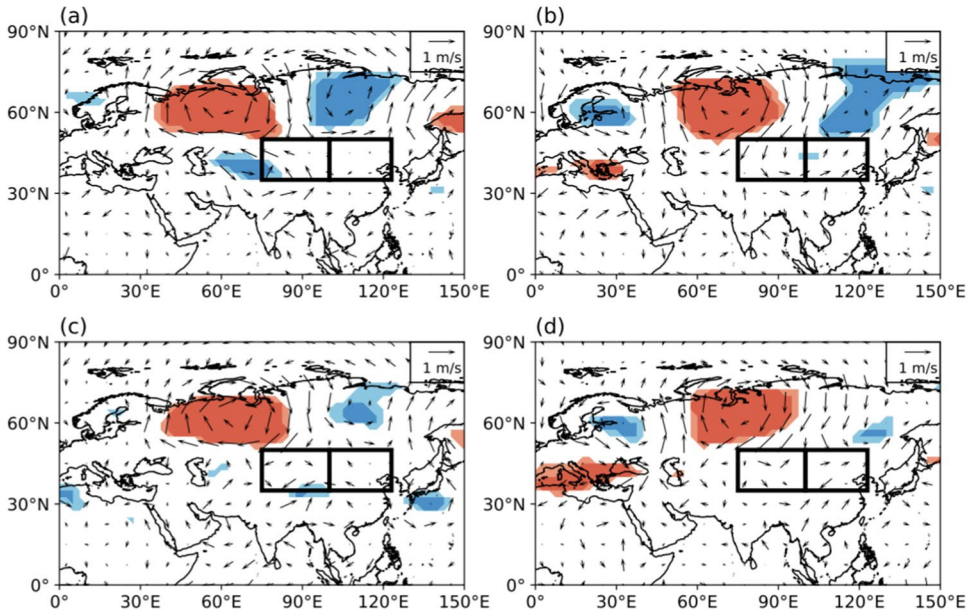

Fig. 11 Same as Fig. 8, but for BBCI

(Fig. 11a). A negative *Z* anomaly occupies most of NWC with ascending motion (Fig. 12a), beneficial to more precipitation in situ for P1. At 850 hPa, NWC has easterly anomalies (Fig. 11c). During P2 (Fig. 11b), the BBCI-related high-latitude wave train has two positive centers, which are located over the Mediterranean Sea and the Ural Mountains. The two centers of the high-latitude wave train are the main systems affecting the consistency of precipitation anomalies in NWC and NC. The strong anticyclone near the Ural Mountains moves more eastward than during the P1 stage, which is located in 60° N (Fig. 11a, c). The anomalous northeasterly wind from the east side of this anticyclone can transport a large amount of cold and wet air from the Arctic Ocean to NWC and NC. The two regions are occupied by westerly anomalies at 850 hPa (Fig. 11d). Positive 500-hPa *Z* anomalies over the Ural Mountains and the Mediterranean Sea and the East Asia trough that leads the cold air to Northern China modulate the summer precipitation in NWC and NC after early 2000. In addition, the water vapor from low latitudes to NC (Fig. 9d) and anomalous upward motion around NWC are responsible for more summer precipitation in the two regions (Fig. 12b). Fig. 10c and d shows the CCs of the BBCI with the summer rainfall for P1 and P2. During P1, a positive correlation occurs in the southwest of NWC, but it is weak in NC. During P2, the positive correlation becomes strong in NC; the positive correlation in NWC weakens and moves east. The results are the same as in Table 1. Thus, after 2000, the summer precipitation in NWC and NC regions has a significant positive correlation with the BBC pattern.

5 Conclusions and discussion

In this study, we use the CN05.1 data, CRU dataset, and NCEP-NCAR reanalysis dataset to investigate the change in the relationship between summer precipitation variabilities in NWC and NC. The results show that the summer precipitation in NWC and NC increases simultaneously after 2000. The positive correlation became enhanced after the mid-1980s, but the CCs were small and insignificant before 2000. After 2000, the correlation strengthens notably, and the correlation coefficients get largely positive and remarkable. The large-scale atmospheric circulation anomalies are analyzed to understand the possible causes for the change of connection between the summer precipitation variations in the two regions after 2000. During P1, the summer precipitation in NWC is related to SRP and BBC. The CC between SRPI and BBCI with NWCI is – 0.59 and 0.52, respectively. The low pressure and associated cyclonic anomalies and concurrent anomalous upward motion over NWC are responsible for more precipitation in situ. The summer precipitation in NC is only related to SRP, and the CC is 0.59. During P2, the summer precipitation in the two regions positively correlates to the BBC, and the CCs are 0.49 and 0.69, respectively. The *Z* anomalies associated with the summer precipitation in NWC stimulate the downstream dispersion of Rossby wave energy and consequently affect the atmospheric circulation pattern that can cause the negative *Z* anomaly around NWC, accompanying anomalous upward motion. In addition, the southeast wind anomaly in the equatorial Pacific

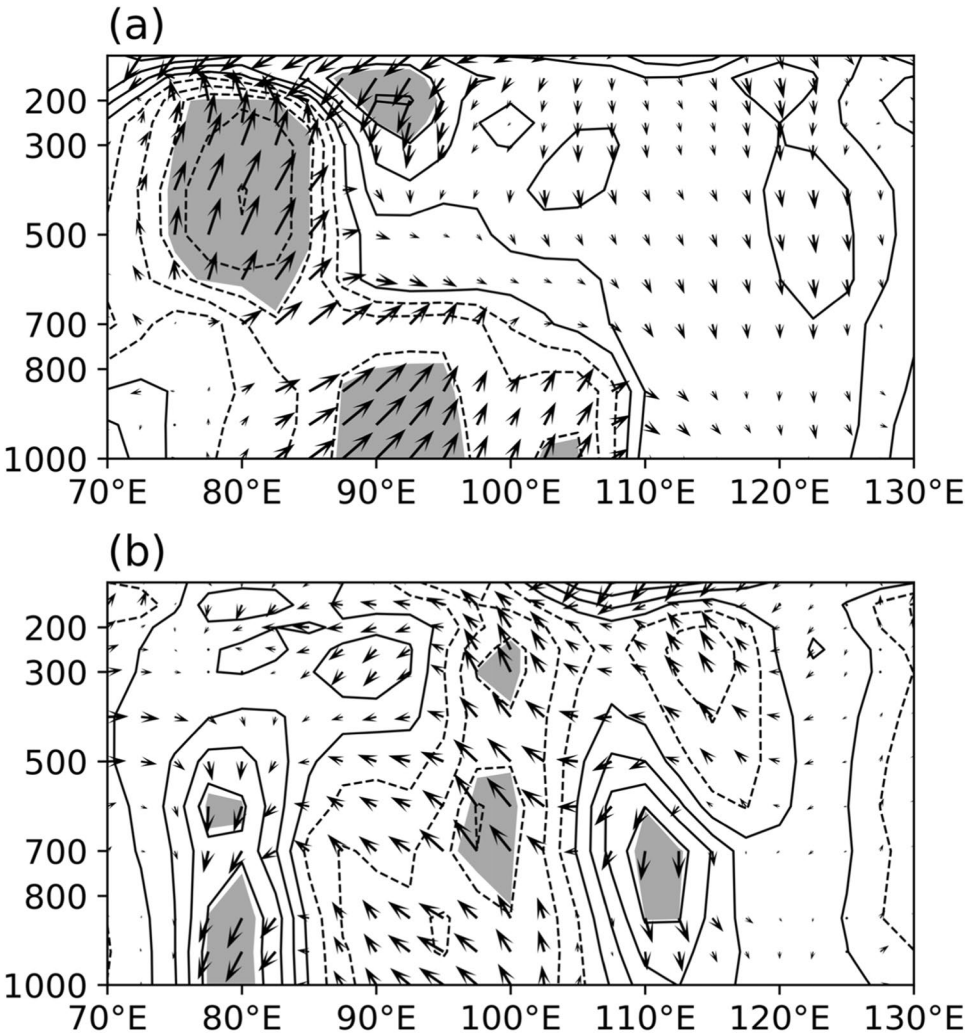

Fig. 12 Regression maps of anomalous JJA omega (contour, contour interval = 0.15, units: m/s) and vertical circulation (vector, synthesis based on u wind and omega, unit: m/s) on a longitude-height cross section along 40° N with respect to BBCI for the periods **a** 1973–1991 and **b** 2000–2018. Shadings indicate the regression coefficients for omega are significant at the 95% confidence level using the two-tailed Student's *t* test

is significantly stronger during P2 than during P1, which can bring moist air from low latitudes to NWC. The positive *Z* anomaly over the Ural Mountains associated with the summer precipitation in NC is enhanced compared to that during P1. To its east side, there is a southward low-pressure trough. This trough forms a closed low pressure in NC, and the anomalous southerly winds bring moist air from the Northwest Pacific to NC. Westerly wind anomalies dominate these two regions.

The SRP mainly affects the summer rainfall in NWC and NC during P1. A positive correlation between the SRPI and summer precipitation anomalies appears in the west of NC, whereas a negative correlation is observed in NWC. However, this correlation is not clear for P2. Summer precipitation in the two regions during P2 is primarily due to the simultaneous modulation of four geopotential height anomalies, which are associated with the BBC pattern over the middle to high latitudes. The East Asia trough leads the cold air to the south and induces westerly winds over NWC and NC. Its southeast is accompanied by a positive *Z* anomaly over Northwest Pacific. The associated southerly wind anomalies on the western flank of the *Z* anomaly can transport water vapor from low latitudes to NC. In addition, significant negative *Z* anomalies over NWC accompany anomalous upward motion around this region. The others are over the Ural blocking high and the positive 500-hPa *Z* anomalies over the Mediterranean Sea, which can affect the positive *Z* anomaly over Northwest Pacific and the negative *Z* anomalies over NWC by the dispersion of Rossby wave energy (Li et al. 2021) and then induce associated precipitation anomalies over NC and NWC. Besides, during the same-sign year of summer rainfall anomaly in NWC and NC, in P2, the BBC pattern was located over mid-high latitudes. However, during P1, SRP teleconnection occurs when concurrent but opposite signed summer precipitation anomalies in NCW and NC are found.

This study concentrates on the change of relation between the summer precipitation variations in the two regions. Furthermore, we have determined the corresponding teleconnection patterns that may affect the change. We analyze the

interannual relationship between NWC and NC from the atmospheric circulation. Changes in the associated atmospheric circulation are the immediate cause of the interannual relationship change between the NWC and NC rainfall. However, the variations of the precipitation in NWC and NC are affected by many factors, including the variation of sea surface temperature (Hoskins and Karoly 1981; Zhang et al. 1999; Alexander et al. 2002; Liu et al. 2007; Piao et al. 2017; Yin and Zhou 2019, 2020), Western Pacific subtropical high (Wu and Qian 1996; Qian et al. 2001b; Sui et al. 2007; Li 2012; Lee et al. 2013), the dynamic and thermodynamic effects of Tibetan Plateau (Wu and Qian 1996, 2003; Qian et al. 2001a, 2001b; Zhang et al. 2004; Zhao et al. 2007), and so on. Therefore, it is worth to examine further the effect of external forcing on the relationship change between the summer precipitation variations of two regions. Previous studies have pointed out that ENSO can affect the summer precipitation in NWC and NC by influencing the East Asian summer monsoon and atmospheric teleconnection since the 1990s (Hoskins and Karoly 1981; Rasmusson and Wallace 1983; Zhang et al. 1999; Wang et al. 2000; Alexander et al. 2002; Piao et al. 2017). The tropical sea surface temperature is recognized as a critical external force that impacts summer rainfall variability in the two regions. This study found that the interannual relationship change between NWC and NC appeared in early 2000. Hu et al. (2020) suggested that the ENSO variability and frequency decrease and increase in 1999/2000, respectively. Whether the change of ENSO will affect the precipitation relationship change between the two regions remains to be studied.

In addition, NWC and NC are located in the arid and semi-arid regions of East Asia. The westerly and monsoons directly impact these two regions (Liu and Zhang 2013; Zhang et al. 2016; Xing and Wang 2017). Therefore, it is necessary to clarify further the influence mechanism of the monsoon and westerly circulation. Besides, the influence of the westerly-monsoon interaction on the relationship between the summer precipitation variations in the two regions remains to be studied.

The present research has not focused on numerical model experiments. The numerical model experiments will be used in the future to further confirm the linkage of summer precipitation between NWC and NC.

Author contribution All the authors contributed to conceptualize and design the study. Data were gathered by Zhaoyang Du; an initial draft of the paper was prepared by Zhaoyang Du; the article was repeatedly revised to generate the final version by Lian-Tong Zhou and Xiaoxue Yin.

Funding This study was funded by the National Natural Science Foundation of China (grant no. 42105063).

Data availability The authors thank Dr. Jie Wu for providing the CN05.1 data. Other data that support the findings of this study are openly available online. The CRU data are freely available at https://crudata.uea.ac.uk/cru/data/hrg/. The NECP-NCAR reanalysis data are freely available at https://psl.noaa.gov/data/reanalysis/reanalysis.shtml.

Code availability The codes used for the processing of data can be provided on request to the corresponding author.

Declarations

Ethics approval and consent to participate Not applicable.

Consent for publication All the authors consented to publish the paper.

Competing interests The authors declare no competing interests.

References

Alexander MA, Bladé I, Newman M, Lanzante JR et al (2002) The atmospheric bridge: the influence of ENSO teleconnections on air–sea interaction over the global oceans. J Clim 15(16):2205–2231

Chen D, Dai Y (2009) Characteristics and analysis of typical anomalous summer rainfall patterns in Northwest China over the last 50 years. Chinese J Atmospheric Sci (in Chinese) 33(06):1247–1258

Chen G, Huang R (2012) Excitation mechanisms of the teleconnection patterns affecting the July precipitation in Northwest China. J Clim 25(22):7834–7851

Chen Y, Zhai P (2015) Synoptic-scale precursors of the East Asia/Pacific teleconnection pattern responsible for persistent extreme precipitation in the Yangtze River valley. Q J R Meteorol Soc 141(689):1389–1403

Chen W, Zhu D, Liu H, Sun S (2009) Land-air interaction over arid/semi-arid areas in China and its impact on the east Asian summer monsoon. Part I: calibration of the land surface model (BATS) using multicriteria methods. Adv Atmos Sci 26(6):1088

Ding Q, Wang B (2005) Circumglobal teleconnection in the Northern Hemisphere summer. J Clim 18(17):3483–3505

Gong Z, Feng G, Dogar MM, Huang G (2018) The possible physical mechanism for the EAP–SR co-action. Clim Dyn 51(4):1499–1516

Harris I, Jones PD, Osborn TJ et al (2014) Updated high-resolution grids of monthly climatic observations-The CRU TS3. 10 dataset. Int J Climatol 34(3):623–642

Han L, Zhang Q, Jian J et al (2019) Drought severity, frequency, duration and regional differences in China. J Desert Res (in Chinese) 39(5):1–10

Hao L, Ding Y (2012) Progress of precipitation research in North China. Prog Geogr (in Chinese) 31(5):593–601

Hoskins B, Karoly D (1981) The steady linear response of a spherical atmosphere to thermal and orographic forcing. J Atmos Sci 38(6):1179–1196

Hu ZZ, Kunar A, Huang BH et al (2020) The interdecadal shift of ENSO properties in 1999/2000: a review. J Clim 33(11):4441–4462

Huang G (2004) An index measuring the interannual variation of the East Asian summer monsoon—the EAP index. Adv Atmos Sci 21(1):41–52

Huang R, Xu Y, Zhou L (1999) The interdecadal variation of summer precipitation in China and the drought trend in North China. Plateau Meteopology (in Chinese) 18(4):465–476

Huang R, Gu L, Chen J, Gang H (2008) Recent progresses in studies of the temporal-spatial variations of the east asian monsoon system and their impacts on climate anomalies in China. Chin J Atmos Sci (in Chinese) 32(004):691–719

Huang G, Liu Y, Huang R (2011) The interannual variability of summer rainfall in the arid and semiarid regions of Northern China and its association with the Northern Hemisphere circumglobal teleconnection. Adv Atmos Sci 28(2):257–268

Huang J, Ji M, Liu Y et al (2013) An overview of arid and semi-arid climate change. Prog Inquisitiones DE Mutatione Clim (in Chinese) 9(01):9–14

Huang J, Chen W, Wen Z et al (2019) Review of Chinese atmospheric science research over the past 70 years: climate and climate change. Sci China Earth Sci 62(10):1514–1550

Jiang D, Wang H (2005) The natural attributes of East Asian summer monsoon weakening interdecadal in the late 20th century. Chin Sci Bull (in Chinese) 50(020):2256–2262

Jin L, Fu J, Chen F et al (2005) Spatial differences of precipitation over Northwest China during the last 44 years and its response to global warming. Sci Geogr Sin (in Chinese) 25(05):567–572

Kalnay E, Kanamitsu M, Kistler R et al (1996) The NCEP/NCAR 40-year reanalysis project. B AM Meteorol Soc 77(3):437–472

Kosaka Y, Xie SP, Nakamura H (2011) Dynamics of interannual variability in Summer precipitation over East Asia. J Clim 24(20):5435–5453

Lee S, Seo Y, Ha K, Jhun J (2013) Impact of the western North Pacific subtropical high on the East Asian monsoon precipitation and the Indian Ocean precipitation in the boreal summertime. Asia-Pac J Atmos Sci 49(2):171–182

Li S (2012) China's huge investment on water facilities: an effective adaptation to climate change, natural disasters, and food security. Nat Hazards 61(3):1473–1475

Li D, Li W, Ying C et al (2003) The present facts and the future tendency of the climate change in Northwest China. J Glaciol Geocryol (in Chinese) 25(02):135–142

Li B, Chen Y, Chen Z et al (2016) Why does precipitation in Northwest China show a significant increasing trend from 1960 to 2010? Atmos Res 167:275–284

Li J, Zheng F, Sun C et al (2019) Pathways of influence of the Northern Hemisphere mid-high latitudes on East Asian climate: a review. Adv Atmos Sci 36(9):902–921

Li D, Liu G, Wu R et al (2021) Co-variability of July precipitation between North China and the Kazakhstan-Xinjiang region and its precursory atmospheric signals. Atmos Res 247(16):105237

Lin Z, Lu R, Wu R (2017) Weakened impact of the Indian early-summer monsoon on North China rainfall around the late 1970s: role of basic state change. J Clim 30(19):7991–8005

Liu H, Ding Y (2011) The interdecadal variability of summer precipitation over North China. J Appl Metorological Sci (in Chinese) 22(2):129–137

Liu L, Zhang D (2013) Spatio-temporal variation of annual precipitation in China and its relationship with the East Asian summer monsoon. Quat Sci 33(01):97–107

Liu D, Dong A, Lu D (2005) Climatic change of Northwest China and its influence on agricultural production in recent 43 years. Agric Res Arid Areas (in Chinese) 23(02):195–201

Liu Q, Wu S, Yang J (2007) A review about coupled ocean-atmosphere dominating modes in three tropical oceans and their interactions. Acta Meteorol Sin (in Chinese) 29(1):1–6

Liu Y, Zhang X, Sun Y (2011) Spatiotemporal variations of rainy season precipitation in Northwest China arid region under global warming. Adv Clim Change Res (in Chinese) 7(02):97–103

Liu W, Zhang Q, Fu Z (2017) Variation characteristics of precipitation and its affecting factors in Northwest China over the past 55 years. Plateau Meteopology (in Chinese) 36(06):1533–1545

Liu Y, Zhou W, Qu X, Wu R (2020) An interdecadal change of the boreal summer Silk Road Pattern around the late 1990s. J Clim 33(16):7083–7100

Lu R, Oh J, Kim B (2002) A teleconnection pattern in upper-level meridional wind over the North African and Eurasian continent in summer. Tellus A: Dyn Meteorol Oceanogr 54(1):44–55

Ma P, Yang J, Lu G et al (2020) The transitional change of climate in the east of Northwest China. Plateau Meteopology (in Chinese) 39(04):840–850

Mo X, Xia J, Hu S, Lin Z (2016) Influences of climate changes on agricultural water resources in North China Plain. Chin J Nat (in Chinese) 38(03):189–192

Murakami M (1979) Large-scale aspects of deep convective activit over the GATE area. Mon Wea Rev 107(8):994–1013

Nitta T (1987) Convective activities in the tropical Western Pacific and their impact on the Northern Hemisphere summer circulation. J Meteorol Soc Japan 65(3):373–390

Peng D, Zhou T (2017) Why was the arid and semiarid Northwest China getting wetter in the recent decades? J Geophys Res 122(17):9060–9075

Piao J, Chen W, Wei K et al (2017) An abrupt rainfall decrease over the Asian inland plateau region around 1999 and the possible underlying mechanism. Adv Atmos Sci 34(4):456–468

Qian Z, Wu T, Liang X (2001) Feature of mean vertical circulation over the Qinghai-Xizang plateau and its neighborhood. Chin J Atmos Sci (in Chinese) 25(4):444–454

Qian Z, Wu T, Song M et al (2001) Arid disaster and advances in arid climate researched over Northwest China. Adv Earth Sci (in Chinese) 6(01):28–38

Rasmusson EM, Wallace JM (1983) Meteorological aspects of the El Niño/Southern Oscillation. Science 222(4629):1195

Ren Z, Yang D (2007) Trend and characteristics of climatic change in arid region of Northwest China in resent 50 years. J Earth Sci Environ (in Chinese) 29(1):99–99

Ren G, Guo J, Xu M et al (2005) Climate changes of Chinese mainland over the past half century. Acta Meteorol Sin (in Chinese) 63(06):942–956

Shang W, Li S, Ren X, Duan K (2020) Event-based extreme precipitation in Central-Eastern China: large-scale anomalies and teleconnections. Clim Dyn 54(3–4):2347–2360

Shi Y, Shen Y, Hu R (2002) Preliminary study on signal, impact and foreground of climatic shift from warm-dry to warm-humid in Northwest China. J Glaciol Geocryol (in Chinese) 24(03):4–11

Shi Y, Shen Y, Li D et al (2003) Discussion on the present climate change from warm-dry to warm-wet in Northwest China. Quat Sci (in Chinese) 23(02):152–164

Song L, Zhang C (2003) Changing features of precipitation over Northwest China during the 20th century. J Glaciol Geocryol (in Chinese) 25(02):143–148

Sui C, Chung P, Li T (2007) Interannual and interdecadal variability of the summertime western North Pacific subtropical high. Geophys Res Lett 34(11):L11701

Sun X, Xu Y, Zhang Z, Yang X (2019) The tropical and extratropical-origin summer meridional teleconnections over East Asia. Clim Dyn 53(1–2):1–15

Tang G, Lin X (2007) The dipole relationship between the summer precipitation over Northwest and North China and its circulation features. Plateau Meteopology (in Chinese) 26(05):901–909

Wang C (2019) Three-ocean interactions and climate variability: a review and perspective. Clim Dyn 53(7):5119–5136

Wang Z, Ding Y (2008) Climatic characteristics of rainy seasons in China. Chin J Atmos Sci 32(01):1–13

Wang B, Wu R, Fu X (2000) Pacific-East Asian teleconnection: how does ENSO affect East Asian climate? J Clim 13(9):1517–1536

Wang C, Wang S, Yang D et al (2001) Studies on basic and anomaly features of precipitation during spring in Northwest China. J Lanzhou Univ (Natural Sciences) 37(03):104–111
Wang X, Xu X, Miao Q (2003) Regional characteristics of summer precipitation and water vapor amount in Northwest China. Clim Environ Res (in Chinese) 8(01):35–42
Wang Y, Chen W, Zhang J (2012) Interannual variations of summer rainfall and their causes in the mid-latitude arid/semi-arid areas of East Asia. Clim Environ Res 17(4):444–456
Wang Y, Chen W, Zhang J, Nath D (2013) Relationship between soil temperature in may over Northwest China and the East Asian summer monsoon precipitation. Acta Meteor Sin 27(5):716–724
Wang L, Xu P, Chen W, Liu Y (2017) Interdecadal variations of the Silk Road Pattern. J Clim 30(24):9915–9932
Wang T, Luo Y, Zhong Y, Zheng W (2017) Comparison of recent precipitation tendency between Northwest and North China. J China Hydrol (in Chinese) 37(1):56–63
Wei Z, Chen W, Huang R (2010) Vertical atmospheric structure and boundary layer height in the summer clear days over Dunhuang. Chin J Atmos Sci (in Chinese) 34(0 5):905–913
Wei W, Zhang R, Yang S et al (2019) Quasibiweekly oscillation of the South Asian high and its role in connecting the Indian and East Asian summer rainfalls. Geophys Res Lett 46(6):14742–14750
Wu R (2002) A mid-latitude Asian circulation pattern in boreal summer and its connection with the Indian and East Asian summer monsoons. Int J Climatol 22(15):1879–1895
Wu R (2017) Relationship between Indian and East Asian summer rainfall variations. Adv Atmos Sci 34(1):4–15
Wu J, Gao X (2013) A gridded daily observation dataset over China region and comparison with the other datasets. Chin J Geophys (in Chinese) 56(04):1102–1111
Wu T, Qian Z (1996) The comparative analyses of differences between vertical circulation on north side of Tibetan Plateau in wet and dry summer and thermal effects of the plateau. Acta Meteorol Sin (in Chinese) 54(6):558–568
Wu T, Qian Z (2003) The relation between the Tibetan winter snow and the Asian summer monsoon and rainfall: an observational investigation. J Clim 16(12):2038–2051
Xing W, Wang B (2017) Predictability and prediction of summer-rainfall in the arid and semi-arid regions of China. Clim Dyn 49(1–2):419–431
Xu P, Wang L, Chen W (2018) The British-Baikal Corridor: a teleconnection pattern along the summertime polar front jet over Eurasia. J Clim 32(3):877–896
Yang X, Xie Q, Zhu Y et al (2005) Decadal-to-interdecadal variability of precipitation in North China and associated atmospheric and oceanic anomaly patterns. Chin J Geophys (in Chinese) 48(04):789–797
Yang Q, Ma Z, Fan X et al (2017) Decadal modulation of precipitation patterns over East China by sea surface temperature anomalies. J Clim 30(17):7017–7033
Yang R, Xing P, Du W et al (2020) Climatic characteristics of precipitation in North China from 1961 to 2017. Sci Geogr Sin 40(9):1573–1583
Yang J, Zhang Q, Lu G et al (2021) Climate transition from warm-dry to warm-wet in Eastern Northwest China. Atmosphere 12(548):2073–4433
Yin X, Zhou L (2019) An interdecadal change in the influence of the Central Pacific ENSO on the subsequent north tropical Atlantic spring SST variability around the mid-1980s. Clim Dyn 53(1):879–893
Yin X, Zhou L (2020) Strengthened relationships of Northwest China wintertime precipitation with ENSO and midlatitude North Atlantic SST since the mid-1990s. J Clim 33(10):3967–3988
Yu S, Lin X, Xu X (2003) The climatic change in Northwest China in recent 50 years. Clim Environ Res (in Chinese) 8(01):9–18
Zhang R, Akimasa S, Masahide K (1999) A diagnostic study of the impact of El Niño on the precipitation in China. Adv Atmos Sci 16(2):229–241
Zhang Y, Li T, Wang B (2004) Decadal change of the spring snow depth over the Tibetan Plateau: the associated circulation and influence on the East Asian summer monsoon. J Clim 17(14):2780–2793
Zhang H, Zhang Q, Yue P et al (2016) Aridity over a semiarid zone in Northern China and responses to the East Asian summer monsoon. J Geophys Res Atmos 121(23):13901–13918
Zhang Q, Lin J, Liu W, Han L (2019) Precipitation seesaw phenomenon and its formation mechanism in the eastern and western parts of Northwest China during flood season. Sci China Earth Sci (in Chinese) 049(012):2064–2078
Zhang Q, Yao Y, Li Y et al (2020) Progress and prospect on the study of causes and variation regularity of droughts in China. Acta Meteorol Sin (in Chinese) 78(03):500–521
Zhao P, Zhou Z, Liu J (2007) Variability of Tibetan spring snow and its associations with the hemispheric extratropical circulation and East Asian summer monsoon rainfall: an observational investigation. J Clim 20(15):3942–3955
Zhao C, Wang Y, Ding Y (2011) Spatial-temporal variations of temperature and precipitation in Northern China in recent 50 years. Plateau Meteopology (in Chinese) 30(2):385–390
Zhao Y, Wang M, Huang A et al (2014) Relationships between the West Asian subtropical westerly jet and summer precipitation in northern Xinjiang. Theor Appl Climatol 116:403–411
Zhao G, Jiang B, Wang Y, Shen X (2017) Characteristics of summer water vapor transport in the eastern Northwest China and their relationships with precipitation. Arid Land Geogr (in Chinese) 040(2):239–247
Zhou W, Chan JCL (2007) ENSO and South China Sea summer monsoon onset. Int J Climatol 27(2):157–167
Zhou L, Huang R (2003) Research on the characteristics of interdecadal variability of summer climate in China and its possible cause. Clim Environ Res (in Chinese) 8(03):274–290
Zhou L, Huang R (2006) Characteristics of interdecadal variability of the difference between surface temperature and surface air temperature in spring in arid and semi-arid region of Northwest China and its impact on summer precipitation in North China. Clim Environ Res (in Chinese) 11(1):1–13
Zhou F, Zhang R, Han J (2019) Relationship between the circumglobal teleconnection and Silk Road Pattern over Eurasian continent. Sci Bull 64(6):374–376